

Ultraviolet-laser induced desorption of NO from the Cr₂O₃(0001) surface: Involvement of a precursor state?

M. Wilde and O. Seiferth

Fritz-Haber-Institut der Max-Planck-Gesellschaft, Faradayweg 4–6, D-14195 Berlin, Germany

K. Al-Shamery

Physikalische Chemie, Carl v. Ossietzky University, Postfach 2503, D-26111 Oldenburg

H.-J. Freund

Fritz-Haber-Institut der Max-Planck-Gesellschaft, Faradayweg 4–6, D-14195 Berlin, Germany

(Received 6 October 1998; accepted 22 April 1999)

NO molecules interact with the Cr₂O₃(0001) surface to form a chemisorption bond of 1.0 eV. At higher coverages an additional more weakly bound species appears in thermal desorption spectra with a binding energy of 0.35 eV. By infrared spectroscopy the weakly adsorbed species is identified to be an unusually strong bound NO-dimer exhibiting a weak feature at 1857 cm⁻¹ beside the chemisorbate absorption band at 1794 cm⁻¹. Laser induced desorption experiments performed at 6.4 eV are presented with main emphasis on the high coverage regime. The desorbing molecules are detected quantum state selectively using resonance enhanced multiphoton ionization. The desorbing molecules are strongly rotationally and vibrationally excited conform with a nonthermal excitation process. The velocity distributions of single rovibronic states of desorbing NO are bimodal and exhibit a strong coupling of rotation and translation. With increasing coverages an additional channel is observed appearing in the time-of-flight spectra of $v''=0$ as smoothly increasing intensity at long flight times. The numeric values of these unusually long flight times are indicative for long residence times on the surface rather than small kinetic energies. The desorption efficiencies weakly depend on the concentration and vibrational state ranging from $(2.0 \pm 0.3) \times 10^{-17}$ cm² at low coverages to $(1.0 \pm 0.4) \times 10^{-17}$ cm² at high coverages for $v''=0$. The intensity of the desorption signal per laser pulse only increases proportional to the chemisorbate coverage. The data are interpreted assuming the dimers to act as extrinsic precursors within the desorption process.

© 1999 American Institute of Physics. [S0021-9606(99)72027-1]

I. INTRODUCTION

The dynamics of laser induced reactions at surfaces after electronic excitation has been the subject of intense study over several decades by now.^{1–3} Of particular interest is the initial excitation and the energy transfer between the molecule and the surface and to internal degrees of freedom.

Very common is an excitation mechanism implying a charge transfer within the adsorbate-surface complex.^{4–6} After excitation the molecule can gain momentum perpendicular to the surface from acceleration within the hyperpotential of the excited state. In most cases, the residence time within the excited state is rather short, for metals a few and for insulator surfaces a few tens of femtoseconds.^{7–9} Depending on the lifetime within the excited state the gain of momentum may be sufficient to overcome the potential well after relaxation into the ground state and thus to initiate desorption. In most cases reported so far, more than one molecular degree of freedom is relevant for the desorption dynamics beside the molecule surface distance.

The dynamics are complicated in the case that temporal trapping of the molecule occurs prior to desorption. In this case, the molecule loses sufficient energy by colliding with the surface to be unable for an immediate escape from the gas-surface potential. During a certain residence time, energy

may be accumulated in excess of the well depth so that the molecules can finally escape and desorb. The phenomenon of trapping or caging prior to desorption has frequently been observed in several photodesorption experiments.^{10–13} In those cases, internal state distributions after desorption normally exhibit two channels, one hot channel resulting from direct desorption and a second channel attributed to trapping with internal state distributions accommodated to the surface temperature.

However, it may come as a surprise that no examples for laser induced desorption have been reported so far which discuss trapping into an intermediate molecular state different from the initial state before laser excitation. Such a process would involve rather complex hyperpotential surfaces with more than one local minimum within the coordinate of the molecule-surface distance in the ground state.

The involvement of such multiple hyperpotentials are well known for describing adsorption and led to the concept of weakly bound precursors preceding chemisorption on solid surfaces in the fifties.^{14–16} Since then it has become an important issue, for example, in the studies of adsorption kinetics using scattering techniques.¹⁷ Two different cases are distinguished. An intrinsic precursor state runs through initial physisorption on a clean surface followed by chemisorption. The model for an extrinsic precursor in adsorption

assumes that molecules adsorbed in a second layer are able to move freely until they reach a vacant adsorption site on the surface and are finally trapped within the chemisorbate state.¹⁶

As mentioned, numerous examples for the involvement of precursors have been reported within investigations on adsorption while none is known for the involvement of a precursor state in UV-laser induced desorption. In this context NO on Cr₂O₃(0001) is a particularly interesting system to study as it exhibits a variety of molecular phases. By controlling the coverage, we have the opportunity to look at the photochemistry of isolated molecules interacting strongly with the surface or to study the high coverage regime where an additional more weakly adsorbed species coexists.

In this paper, we present in the first part a detailed characterization of the NO adsorbed on an epitaxial film of Cr₂O₃(0001) grown on Cr(110) including infrared reflection absorption spectra (IRAS) and temperature programmed desorption (TPD) ranging from low to high coverages. We shall show that the physisorbed species is due to dimer formation at higher coverages. In the second part of the paper, quantum state selective experiments on the UV-laser induced desorption are reported after excitation at 6.4 eV. From recent investigations, it is known that photodesorption of NO at Cr₂O₃(0001) is initiated by an electron transfer from the substrate to the adsorbate with the formation of an NO⁻ like intermediate state from low coverages for the excitation wavelengths used.^{18–21} In this paper, the main emphasis will be put on desorption from the high coverage regime. The data are discussed suggesting a mechanism in which the dimers act as a precursor state within the photoreaction process.

A variety of other interesting phenomena observed in the laser induced desorption of NO/Cr₂O₃(0001) which occur at lower excitation energies such as surface state induced processes and connected electron spin effects are discussed elsewhere.^{18–20} Likewise, the role of the initial vibrational population as well as the influence of hindered translations is subject of further publications.^{20,21}

II. EXPERIMENTAL SETUP

The experiments were carried out in a ultrahigh vacuum (UHV) chamber which has been described in detail previously.²² The system was equipped with low-energy electron diffraction (LEED), Auger electron spectroscopy (AES), x-ray photoelectron spectroscopy (XPS), x-ray Auger electron spectroscopy (XAES), and a TPD facility. Infrared spectra were recorded in a different UHV chamber described elsewhere, equipped with a Mattson Fourier-transform infrared spectrometer (FTIR) with 2 cm⁻¹ resolution.²³ A (110)-terminated chromium single crystal was connected with tantalum rods to a sapphire attached to a copper liquid nitrogen reservoir which allowed cooling to 90 K. The sample temperature was controlled by a chromel-alumel thermocouple spot welded to the side of the crystal. Several cycles of neon ion bombardment and annealing were necessary to clean the crystal from contamination mainly due to atomic nitrogen. An epitaxial film of Cr₂O₃(0001) of 30–50 Å thickness was obtained by oxidizing the cleaned crystal in an atmosphere of

10⁻⁶ Torr of oxygen at 600–800 K and annealing the oxide to 1000 K. To remove contamination the sample was cleaned prior to each experiment by flash heating to 1000 K.

The laser induced desorption (LID) experiments were of pump-probe type. Desorbing NO molecules were detected using resonance enhanced multiphoton ionization (REMPI). The adsorbates were desorbed by pump laser pulses of a broadband excimer laser (Lambda Physik EMG 200) run at 6.4 eV with normal incidence on the surface. The laser fluence was typically 1 mJ/cm² per pulse in most of the experiments with a pulse length of 15 ns. The desorbing molecules were detected in the gas phase after a well-defined time delay at a distance *r* of 32 mm parallel to the surface with an excimer laser (XeCl, Lambda Physik LPX 205 i cc) pumped tunable dye laser (Lambda Physik LPD 3002). For the NO detection, the well-known (1+1) REMPI scheme via the A²Σ state was employed.²⁴ The ions were detected perpendicular to the desorption and detection laser beam direction with a repeller electrode, a short drift tube, microchannel plates and a phosphor screen.

Time-of-flight (TOF) spectra were obtained for single rovibronic states of the NO by fixing the detection laser wavelength to the maximum of a selected rovibronic transition and varying the time delay between desorption and detection laser pulses. At each time delay, the desorption signal was averaged over 150 laser pulses to yield a good signal-to-noise ratio. The transformation into velocity distributions *P*(*v*) was performed by weighting the measured signal *S*(*r*,*t*) with the flight time *t*. The corresponding velocity *v* was calculated from the distance *r* of the detection laser to the surface and the flight time *t*.

The NO molecules were redosed after each desorption laser pulse using a pulsed molecular beam apparatus for the low coverage regime (electromagnetic solenoid valve, General Valve Corporation, driver pulse width 700 μs, NO stagnation pressure=2.0 bar, nozzle diameter=800 μm). The repetition rate of the experiment cycles was 4 Hz. Details of the molecular beam will be given elsewhere.²⁰ Under these conditions, one beam pulse contained approximately 7 × 10⁻⁴ ML of NO, as calibrated against the thermodesorption signal intensity of NO assuming a sticking probability of one (≅ lower limit). The base pressure in the chamber did not exceed 3 × 10⁻¹⁰ Torr when the molecular beam was running.

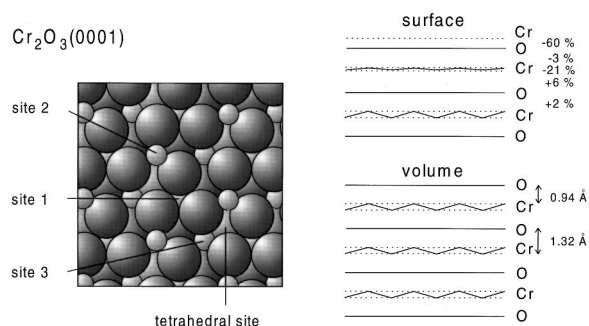
To conduct photodesorption experiments at higher NO coverages background gas dosing was necessary in order to redose a larger number of molecules between the desorption laser pulses. Therefore, the detection laser was operated at twice the desorption laser frequency (2 Hz) and the background signal due to the gas phase NO recorded between the desorption pulses was then easily subtracted using a boxcar integrator.

III. RESULTS

A. The NO adsorption on Cr₂O₃(0001)

1. The clean oxide surface

Chromium oxide is a corundum-type oxide. The stacking of layers along a direction perpendicular to the (0001) plane

FIG. 1. Schematic drawing of the $\text{Cr}_2\text{O}_3(0001)$ surface.

consists of basically flat oxygen layers alternating with buckled metal ion layers. In principle, the polar bulk truncated (0001) surface is electrostatically unstable due to the divergence of the surface potential. A stable (0001) surface is obtained by cutting the stack of layers between the buckled metal ion layer halving the number of metal ions left on the surface (Fig. 1). Further strong relaxation of the first four layers reduces the surface dipole moment and leads to surface energies close to those for nonpolar oxide surfaces as has been found in recent full dynamical LEED studies.²⁵

2. TPD data of NO desorption from $\text{Cr}_2\text{O}_3(0001)$

In order to get insight into the bonding of NO, a series of TPD spectra of NO/ $\text{Cr}_2\text{O}_3(0001)$ was recorded. Figure 2 shows a selection of TPD spectra as a function of increasing NO coverage deposited with the molecular beam doser at 90 K. The temperature ramp of 3 K/s was linear over the whole temperature range. At low coverages, a chemisorbed species is observed at a desorption temperature of (340 ± 20) K. As the peak position of the TPD signal is not much depending on the surface coverage an assumption of first-order desorption kinetics for the analysis of the chemisorbate appears reasonable. From the analysis of the TPD data, a binding energy of 1.0 eV (97.5 kJ/mol) was obtained according to the method of Redhead using a prefactor of 10^{13} s^{-1} .²⁶ Beside chemisorbed NO desorbing at (340 ± 20) K, an additional more weakly adsorbed species is apparent in the TPD spectra at (125 ± 10) K at larger coverages. The inset of Fig. 2 shows the integral of the TPD intensities of the two main spectral features as a function of dosing time. The graph clearly exhibits the saturation behavior for chemisorbed NO before the growth of the second species starts. The latter will be discussed further below.

Features at $m/e=44$ appear simultaneous to desorption of weakly adsorbed NO for large coverages. $M/e=14$ behaves similar to $m/e=44$. This is indicative for N_2O formation. From IR data it is apparent that the reaction occurs during heating with immediate escape of the N_2O into the gas phase after formation. Apparently, some impurities trigger this reaction during thermal desorption as N_2O is only observed for high dosing rates using background dosing. No N_2O formation occurred with molecular beam dosage for which the background pressure did not exceed 3×10^{-10} Torr.

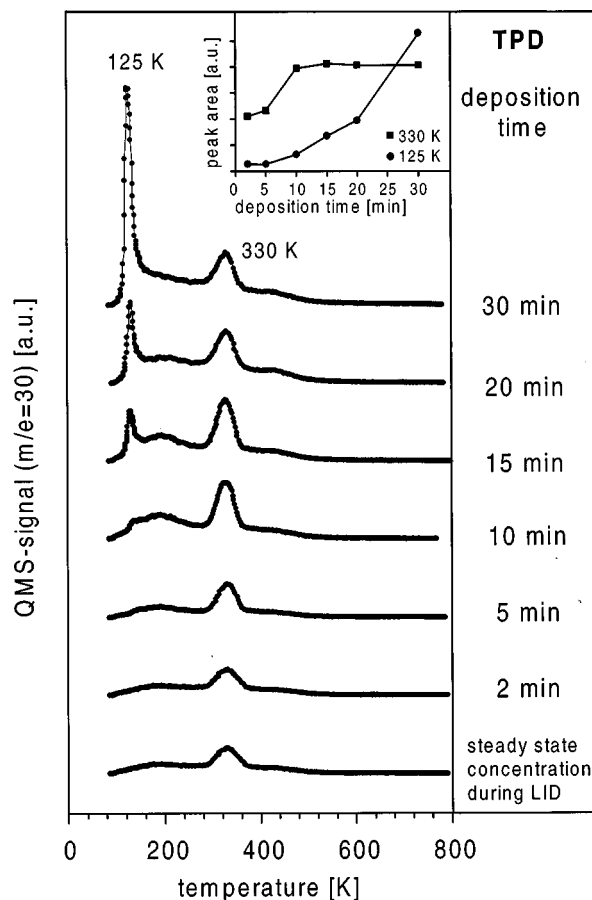


FIG. 2. Temperature programmed desorption spectra (TPD) of NO from $\text{Cr}_2\text{O}_3(0001)$ taken with a linear temperature ramp of 3 K/s for increasing dosing times at 90 K (dosing with a molecular beam: 4 Hz, driver pulse width 700 μs , NO stagnation pressure=2.0 bar, nozzle diameter=800 μm ; lowest trace: equilibrium concentration at surface during LID experiments) (QMS-signal maximum at 340 K $\approx 7 \times 10^{-9}$ A). Inlet: integral intensities of TPD spectra of NO/ $\text{Cr}_2\text{O}_3(0001)$ as a function of deposition duration at 90 K for the two main desorption species.

3. Adsorption of NO: low coverages

The chemisorbed species has intensively been studied by a variety of spectroscopic methods like electron-energy loss spectroscopy (EELS), XPS, angular resolved UV photoelectron spectroscopy (ARUPS), IRAS, and ion scattering spectroscopy (SS).²⁷ The molecule is known to adsorb on top of the chromium ions with a tilt angle of 20° – 40° with respect to the surface normal.²⁷ No superstructure has been observed with LEED suggesting that the adsorbate layer is likely to be disordered and forms a (1×1) superstructure after saturation of the regular chemisorption sites. From photoemission data, it was confirmed that NO substantially covers the surface, in other words that chemisorption is definitely not due to defect adsorption.^{27,28}

The chemisorption energy is remarkably high for a transition metal oxide surface where the bonding is often dominated by electrostatic interactions.²⁹ In case of NO/ $\text{Cr}_2\text{O}_3(0001)$, the adsorption energy is twice as large compared to what has been found for other systems.²⁹ A stronger chemisorptive interaction is also apparent from strong shifts of binding energies of molecular orbitals found in ARUPS, from strong shifts of the vibrational frequency with respect

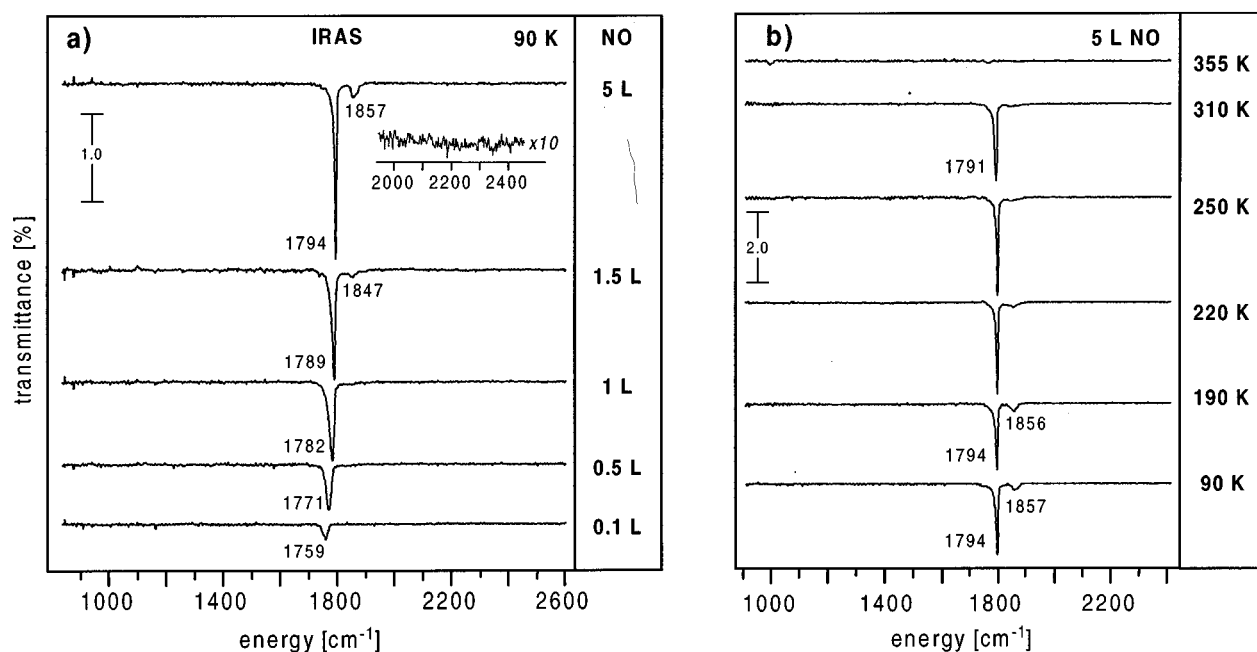


FIG. 3. (a) FTIR spectra of NO/Cr₂O₃(0001) as a function of coverage (dosing via needle doser). (b) FTIR spectra of NO/Cr₂O₃(0001) for a high coverage (dosing via needle doser) after subsequent short heating to different temperatures.

to the gas phase value²⁷ and from the disappearance of a superstructure for the clean chromium oxide surface at 150 K observed in LEED with adsorption of NO.³⁰

In order to obtain a deeper insight into the NO/Cr₂O₃(0001) interaction, IR spectra were recorded as a function of coverage as shown in Fig. 3(a). At 1 L the vibrational frequency is found to be at 1789 cm⁻¹ which is rather different from the gas phase value of 1876.11 cm⁻¹ (Ref. 31) and which is conform with a strong interaction with the substrate. At lower coverages, the absorption band of the NO stretching vibration shows an asymmetric broadening at the low frequency side and a shift of the IR absorption maximum from 1789 to 1759 cm⁻¹ when reducing the coverage from 1 to 0.1 L. Normally, distortions by coupling effects of close lying frequencies from defects or regular adsorption sites of strong absorbers account for asymmetries in the spectra. In the low coverage limit simultaneous occupation of defect and regular sites are likely to occur. In this regime, it is expected that the frequency of defect sites is shifted towards lower frequencies. This has been observed for NO for a variety of systems with stronger 2π* back donation and is eased by metal *d* orbitals lying close in energy.³² However, at larger coverages, this effect is covered by the more important effect of dipole-dipole coupling leading to a further shift towards higher absorption frequencies with increasing coverage and subsequent linewidth narrowing.³³

4. Adsorption of NO: high coverages

The linewidth narrowing of the absorption band is rather pronounced at coverages above 1 L. In contrast to the low coverage regime (0.1–1 L), the frequency shift of the absorption band from 1789 cm⁻¹ at a 1.5 L dosage to 1794 cm⁻¹ at a 2 L dosage is small. Furthermore, a second small peak at 1857 cm⁻¹ is observed. It disappears when heating the sys-

tem above 220 K [Fig. 3(b)]. The maximum intensities of both absorption bands grow further with increasing coverage. The high frequency vibration couples marginally stronger than the one at 1794 cm⁻¹ as it shifts from 1847 (1.5 L) to 1856 cm⁻¹ (2 L).

Sharp bands are typically seen in multilayers of solid NO.³⁴ However, multilayer formation of NO normally occurs at much lower temperatures than the 90 K used in our experiments [NO/Ag(111): 15–40 K,^{11,34–36} NO/Pt(polycryst.): >20 K,³⁷ NO/LiF(001): 50 K,³⁸ NO/MgF₂: 20 K,³⁹ NO, graphite: 30 K.⁴⁰]. Hence, multilayer formation is unlikely the cause of the weakly adsorbed species encountered here.

Data of isotope mixtures on polycrystalline α-Cr₂O₃ taken under ambient conditions showed that the NO oscillators with absorption bands at 1735–1745 and 1865–1875 cm⁻¹ are equivalent and are not related to different adsorption sites.⁴¹ The cited results rule out a second adsorption site with a weak adsorbate-substrate interaction. Such an adsorption would involve a weak dipole moment and a concomitantly weak adsorption band with an IR frequency close to the gas phase value of 1876.11 cm⁻¹.⁴²

Cis-dinitrosyl species (two NO molecules bound to the same chromium ion without dimer formation) are discussed to account for an absorption band at 1755 cm⁻¹ and a weaker band at 1875–1880 cm⁻¹ on silica supported chromium ions.^{42–44} However, the interpretation is controversial and other authors claim cis-dimer formation to occur for this polycrystalline system.^{45,46}

As the Cr-*d*-orbitals are known to be localized,⁴⁷ long range interactions between the NO molecules at equivalent adsorption sites as cause for the appearance of a second feature in IRAS and TDS may be ruled out as this would imply

interactions on distances of 5 Å (= the distance between equivalent surface Cr-atoms).

5. NO dimers

The frequency of 1857 cm^{-1} characterizing the weakly bound NO on $\text{Cr}_2\text{O}_3(0001)$ is very similar to the symmetric stretching frequency of NO dimers (gas phase value: 1860 cm^{-1} ⁴⁸). The corresponding asymmetric stretching frequency of the dimer in the gas phase is known to be at 1788 cm^{-1} . This frequency matches well with the observed frequency of 1794 cm^{-1} at higher coverages.

Symmetry arguments as stretched out in detail by Brown, Gardner and King can be used to determine the orientation of the dimer.³⁴ In the gas phase, NO dimers have a *cis*-planar trapezoidal structure displaying a C_{2v} symmetry. The coupling of the unpaired $2\pi^*$ electrons give a singulett (1A_1) ground state which explains why the trans conformation is much less stable.⁴⁹ There are a number of examples for which this structure is sustained in solids,⁵⁰ matrixes,⁵¹ and on surfaces.^{34,35,52} The N–N–O bond angles are 101.3° in solid NO.⁵⁰ The N–N distance ranges from the rather large value of 2.236 \AA in the gas phase to 2.18 \AA in the solid. This long N–N distance concomitant with the weak dimer bond is attributed to the Pauli repulsion between the electrons in the 1π orbitals of the NO molecules within the dimer plane.

We assume that the usually found *cis*-planar trapezoidal configuration of the dimer is also sustained on $\text{Cr}_2\text{O}_3(0001)$. Even though dipole selection rules principally differ on surfaces of oxides and of metals, screening effects are still possible on thin insulating films due to an underlying metal, so that in a first approximation the metal selection rules are likely to be sustained also on the $30\text{--}50\text{ \AA}$ thin epitaxial chromium oxide film.^{53,54} Therefore, it is unlikely that a rather flat lying dimer would have significant intensities in the vibrations. Furthermore, it is known from *ab initio* calculations on similar systems like NO/NiO(100)⁵⁵ that the interaction of the oxygen $2p$ bands and the 2π system of the NO molecules is strongly repulsive. From both arguments it is very likely that the molecular plane shows a stronger tilt with respect to the surface. The interaction of the dimers with the underlying support is asymmetric, if one chromium ion is involved in the surface bond. The resulting symmetry is either C_s^2 (end on symmetry as depicted in Fig. 4) or C_1 . In both cases, both NO stretching vibrations are allowed from symmetry selection rules. Let us assume a geometry with an end-on symmetry as depicted in Fig. 4. For this packing arrangement, the net dipole moment of the symmetric stretch will be perpendicular to the direction of the N–N bond while it will be parallel to the N–N bond for the asymmetric stretch. As the symmetric stretching vibration at higher frequencies (1857 cm^{-1}) is approximately parallel to the surface the intensity of this vibration remains much weaker in intensity than the corresponding asymmetric stretching vibration (at 1794 cm^{-1}). The case is just the other way round for an adsorption geometry with both N-ends interacting with the surface (“upright” or “tilted,” i.e., with a certain tilt of the molecular plane with respect to the surface”) for which the symmetric stretch would dominate the

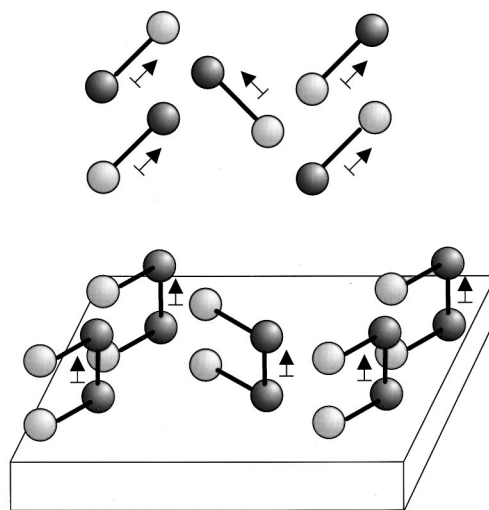


FIG. 4. Schematic drawing of the crystal-packing structure as suggested by Suzanne *et al.* (see Ref. 52) at high coverages of NO on graphite; arrangement of dipole moments for (a) the symmetric stretch of the NO dimer viewed from on-top and (b) the asymmetric stretch viewed from the side of the 3D structure [after a drawing of Brown, Gardener, and King (see Ref. 34)].

spectrum. Therefore, an adsorption geometry close to the end-on stacking arrangement like the crystal-packing structure of NO/graphite depicted in Fig. 4 is very likely to occur or a geometry close to it allowing a tilt of the N–N axis with respect to the surface normal.⁵² The arguments based on NO interaction with the surface via a N–Cr ion bond. The same arguments still hold in case bonding occurs via the oxygen in NO which cannot be ruled out from IR-selection rules.

Such a packing structure could also explain the coverage dependence of the frequencies. Similar to our observations Brown, Gardner, and King observed a loose coupling of the symmetric stretch in the second layer and an initial uncoupling of the asymmetric stretch at low multilayer concentrations in adsorption of isotope mixtures of NO on Ag(111) (Ref. 34) which they related to the end-on stacking arrangement as discussed above.

Anyway, the existence of a dimer at such elevated temperatures as 90 K is very unusual. The desorption temperature of the weakly adsorbed species of NO/ $\text{Cr}_2\text{O}_3(0001)$ corresponds to a binding energy of 0.35 eV as derived from a simple Redhead analysis²⁶ when assuming a prefactor of 10^{13} s^{-1} . However, if the molecule is freely rotating in the transition state for the desorption this factor can be up to 2–3 orders of magnitude larger, in other words the binding energy can even be larger. This is in strong contrast to the dissociation energy of the gas phase dimer at $0.089 \pm 0.005\text{ eV}$.⁵⁶ When interacting with a surface dimers can be stabilized at higher energies as has been shown for NO/Ag(111),^{34,35} NO/Cu(111),⁵⁷ and NO on oxidized Mo(110).⁵⁸ In those cases, dimers exist even at a surface temperature of 90 K. However, this is the exception rather than the rule. Normally, the molecule surface interaction is either so strong that monomer adsorption is preferred or weakly interacting NO molecules dimerise immediately.

Stabilization of the dimer on $\text{Cr}_2\text{O}_3(0001)$ could occur either by an interaction of both NO molecules with the sub-

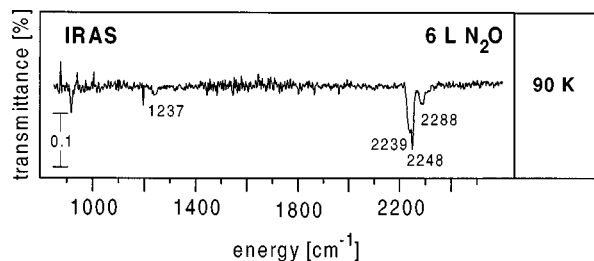


FIG. 5. FTIR spectra of 6 L $\text{N}_2\text{O}/\text{Cr}_2\text{O}_3(0001)$ deposited at 90 K.

strate (which was ruled out from IR intensity arguments) or a substantial change of the Pauli repulsion between the 1π orbitals. This may be caused by either a strong distortion of the electronic structure of the NO end in contact with the substrate or from the strong electric fields of the polar surface.

This kind of perturbed dimers seems to be a peculiarity of certain oxidic surfaces as similar observations have been found by Queeney, Pang, and Friend for NO dimers on oxidized Mo(110).⁵⁸ Dimer formation did not occur on Mo(110) (Ref. 59) and Mo(110) modified with atomic oxygen in high coordination sites,⁶⁰ though both exhibit rich NO spectra in IRAS and high-resolution electron energy loss spectroscopy (HREELS). Supported by elaborate isotopic experiments they attributed a feature at 1871 cm^{-1} to dimer formation on oxidized Mo(110) while a second feature at 1820 cm^{-1} was related to dinitrosyl. A feature at 1728 cm^{-1} belonging to monomeric nitrosyl only marginally shifted to higher frequencies and sharpened with dimer occurrence.

6. N_2O formation?

N_2O formation is observed for a number of systems like the high coverage regime of NO on Si(111)(7×7),⁶¹ NO on Mo(110),⁵⁹ and oxygen modified Mo(110)⁶⁰ or NO dimers on Ag(111).³⁴ N_2O formation does not occur from simple adsorption at $\text{Cr}_2\text{O}_3(0001)$ as is evident when comparing the $\text{N}_2\text{O}/\text{Cr}_2\text{O}_3(0001)$ IR spectrum (Fig. 5) to the high coverage spectrum of NO (Fig. 3). The N_2O spectrum exhibits a prominent feature centered at 2246 cm^{-1} corresponding to the gas phase value of 2224 cm^{-1} (Ref. 62) of the N–N stretching vibration and a feature centered at 1237 cm^{-1} corresponding to the gas phase value of 1285 cm^{-1} (Ref. 31) of the N–O stretching vibration. These features are absent in the NO spectra even after heating the surface. This indicates that N_2O observed in TPD is formed during heating with immediate escape of the molecules into the gas phase. On oxidized Mo(110), N_2O formation evolves via a dinitrosyl intermediate rather than from dimeric species as shown by Queeney, Pang, and Friend.⁵⁸ The lack of N_2O formation during adsorption implies that the photochemistry of the low and high coverage regime can be studied for NO/ $\text{Cr}_2\text{O}_3(0001)$ without the complication of surface reactions and possible subsequent photodissociation of such reaction products. Also no photoreaction products in detectable amounts have been observed in TPD and XPS measurements after photoexcitation. With this respect our data differ from

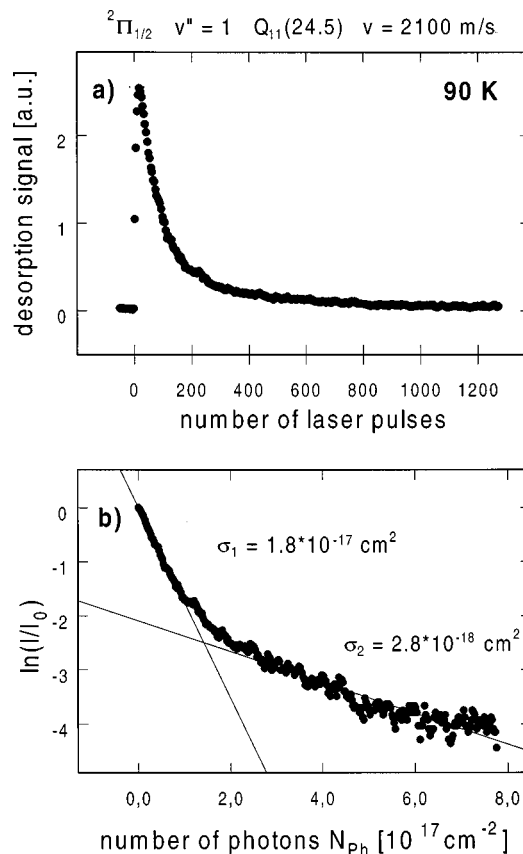


FIG. 6. (a) desorption signal in the gas phase ($v = 2100\text{ m/s}$, $J'' = 24.5$, $v'' = 1$, ${}^2\Pi_{1/2}$) as a function of laser pulses impinging on the surface after preparing a defined initial coverage via molecular beam dosage (5 min dosing at 4 Hz, driver pulse width $700\text{ }\mu\text{s}$, NO stagnation pressure = 2.0 bar , nozzle diameter = $800\text{ }\mu\text{m}$) after LID with 6.4 eV . (b) Evaluation of photodesorption cross sections from the slope of a plot of the logarithm of the intensity of the desorbing species from (a) as a function of the total number of photons n_{ph} impinging on the surface.

other systems such as NO/Si(111)(7×7) for which coverage dependent photochemistry has been studied.⁶¹

B. Photodesorption of NO from $\text{Cr}_2\text{O}_3(0001)$

1. Desorption efficiency

The photodesorption cross sections were measured by preparing a defined initial coverage via molecular beam dosage and a subsequent monitoring of the desorption signal in the gas phase as a function of photons impinging on the surface. Assuming desorption kinetics of first order, the data can be analyzed by plotting the logarithm of the intensity of the desorbing species in a single rovibrational state as a function of the total number of photons n_{ph} impinging on the surface. From the slope the desorption coefficient σ is extracted.

An example for the analysis of the depletion curve starting with a saturation coverage of chemisorbed NO, i.e., a full coverage of regular adsorption sites on $\text{Cr}_2\text{O}_3(0001)$, is shown in Fig. 6. From TPD data it is apparent that the initial surface coverage is substantially depleted depending on the number of photons impinging on the surface. Basically, two slopes can be observed in the semilogarithmic plot of the data. The desorption cross section for coverages exceeding 1/5 of the saturation coverage of the chemisorbate is (2.0

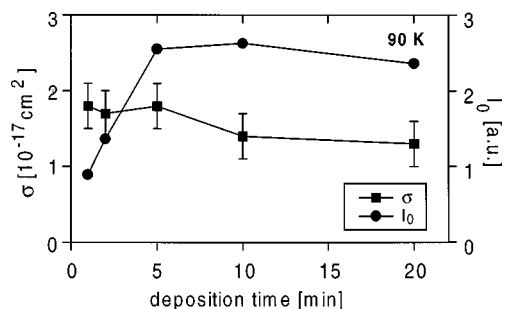


FIG. 7. Desorption cross sections σ (filled squares) and intensity of the initial desorption signal I_0 (filled dots; $J''=24.5$, 2100 m/s, $v''=1$, ${}^2\Pi_{1/2}$) of NO as a function of predosing the $\text{Cr}_2\text{O}_3(0001)$ crystal at 90 K with a molecular beam doser (dosing at 4 Hz, driver pulse width 700 μs , NO stagnation pressure=2.0 bar, nozzle diameter=800 μm) after LID with 6.4 eV.

$\pm 0.3) \times 10^{-17} \text{ cm}^2$, independent of the laser fluence. At coverages below $\sim 1/5$ of the saturation coverage, a desorption cross section of $(2.6 \pm 1.2) \times 10^{-18} \text{ cm}^2$ is measured. The latter can be attributed to defect desorption. This can also be related to our infrared data in which defect influences are apparent for low concentrations within the absorption band of the NO stretching vibration. Since the desorption cross section from coverages with dominating defect adsorption is much smaller than the cross section for higher coverages and NO final state distributions were obtained from measuring at a steady state coverage well above the regime of defect influences (lowest trace, Fig. 2), it is concluded that the phenomena discussed below result from the majority species, i.e., NO at regular adsorption sites.

The desorption efficiency of NO from chromium oxide compares well to measurements on a variety of other oxidic surfaces.³ However, there are some specific state and coverage dependent effects which may be related to the occurrence of two different adsorption species at larger coverages. This will be stretched out in the following paragraph.

By increasing the coverage above saturation of the chemisorption sites the cross section drops by a factor of ~ 1.3 to $(1.5 \pm 0.4) \times 10^{-17} \text{ cm}^2$ in $v''=1$ as soon as the weakly adsorbed species is apparent in TPD. The exact coverage dependence of the desorption cross section is shown in more detail in Fig. 7 together with the initial desorption signal per pulse for $J''=24.5$, 2100 m/s, $v''=1$, ${}^2\Pi_{1/2}$ as a function of the initial dosing with a molecular beam.

The initial desorption signal per pulse remains constant as soon as the chemisorbate species is saturated though the overall coverage can still be further increased. This indicates that the weakly bound species, though influencing the cross section, is not directly involved in the initial excitation step.

As will be discussed further below occurring trapping processes result in thermalization of the vibrational excitation for trapped molecules. Therefore, the observed desorption of NO in $v''=1$ results from the direct desorption channel. Hence, the analysis of the data assuming first order kinetics is justified for this internal state.

Desorption cross sections differ for $v''=0$ from vibrationally excited states for those coverages involving the weak adsorbate state and depends on the time delay after the

excitation event. The cross section is found to be $(1.0 \pm 0.4) \times 10^{-17} \text{ cm}^2$ for $v''=0$ for fast desorption velocities independent of the rotational state. For a delay time of 800 μs , a cross section of $(2.1 \pm 0.6) \times 10^{-17} \text{ cm}^2$ was obtained. Therefore, as the desorption process is more complex for larger coverages for NO in $v''=0$, the given cross sections have to be taken more likely as fitting parameters than being a quantitative description of a first-order kinetics for NO desorption within $v''=0$ though the logarithmic plots are clearly linear within a range of two orders of magnitude even in this case.

The error bars are rather large and single measurements can easily differ by a factor of 2 from the average value. This is a well-known problem for cross-section measurements. However, we have to note that there is a clear trend to smaller desorption probability for NO in the vibrational ground state at fast desorption velocities for larger coverages.

The photon energy dependence discussed elsewhere is indicative for a surface induced desorption process which implies an initial excitation of the substrate followed by a temporal charge transfer to the adsorbate.^{18,20}

The desorption efficiency is temperature dependent. An increase of the desorption cross section by about a factor of 2 is observed in the temperature range of 90 and 260 K. A thermal desorption channel due to the laser induced temperature jump within the surface can be ruled out as the temperature rise within the surface is only a few tens of Kelvin under the experimental conditions, while the desorption temperature of chemisorbed NO with 340 K is 240 K above the surface temperature of 100 K.⁶³ One-dimensional wave packet calculations attributed the increase of desorption efficiency with increasing temperature to the increasing thermal population of higher states of the molecule-surface stretching vibration.²¹

2. Velocity distributions

a. Low coverage regime. NO desorption from low coverages on $\text{Cr}_2\text{O}_3(0001)$ has been intensively studied as published elsewhere.¹⁸⁻²¹ The major findings will be summarized in the following. NO desorbs from $\text{Cr}_2\text{O}_3(0001)$ highly rotationally and vibrationally excited. As can be seen from Fig. 8, the shape of the velocity distributions of NO photo-desorbed from low coverages show a strong dependence on the excitation of the various internal degrees of freedom of the desorbing molecules. They are non-Boltzmann like and bimodal showing a pronounced shift of their maxima towards higher velocities with increasing rotational excitation.²⁰ For low rotational states of $v''=0$ ($J'' \leq 16.5$), the velocity distributions exhibit a further unusual coverage dependent peaking at slow velocities which will be discussed further below. The molecules desorb strongly directed along the surface normal evident from two-dimensional imaging measurements of the angular distributions.²⁰

The rotational-level population distribution obtained from the integral of the velocity distributions can be described by a Boltzmann distribution. A phenomenological rotational temperature of (700 ± 80) K is extracted, independent of the vibrational or spin-orbit state of NO. This degree

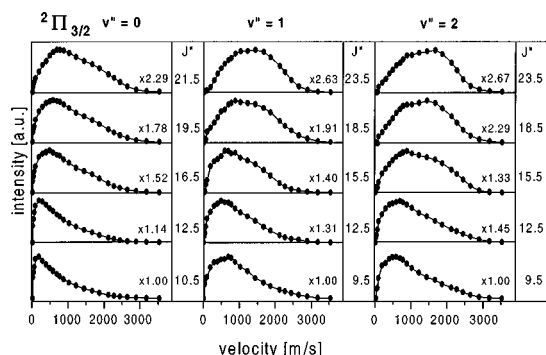


FIG. 8. Velocity distributions of NO desorbing from $\text{Cr}_2\text{O}_3(0001)$ after LID with 6.4 eV as a function of rotational and vibrational ($v''=0,1,2$) excitation of the desorbing molecules in the $^2\Pi_{3/2}$ state (maxima normalized to 1).

of rotational excitation is much larger than in laser desorption products of many other systems.¹⁻³ The Boltzmann plot is shown in Fig. 9(a) for the $^2\Pi_{1/2}$ state as a function of vibrational excitation. A corresponding vibrational temperature of (2900 ± 450) K is obtained from the integral population of the first three vibrational states when averaging over

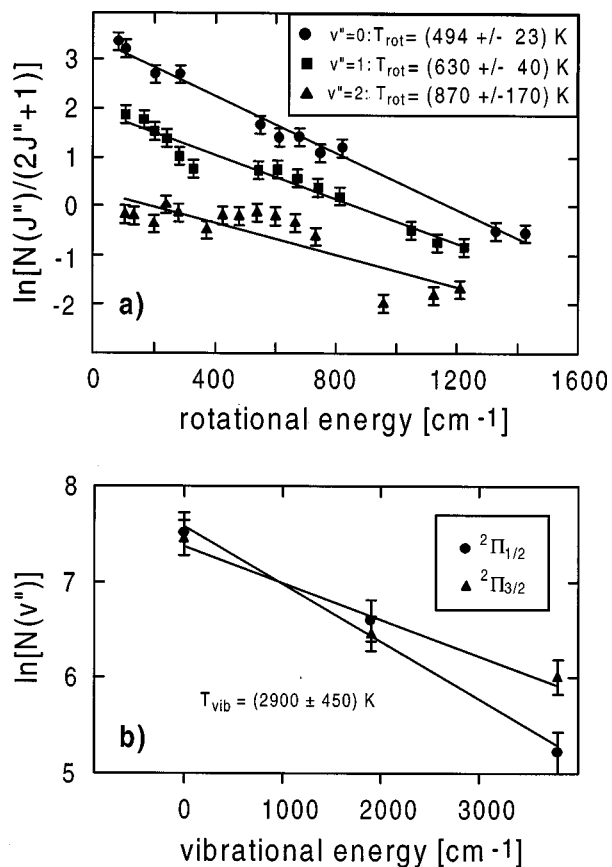


FIG. 9. (a) Evaluation of a phenomenological rotational temperature from a Boltzmann analysis by plotting the logarithm of the integrals of the velocity distributions of NO desorbing from $\text{Cr}_2\text{O}_3(0001)$ after LID with 6.4 eV normalized by the degeneracy factor of the respective rotational state as a function of rotational energy for the first three vibrational states of NO in $^2\Pi_{1/2}$ [$Q_{11} + P_{21}(v''=0,1:450 \text{ m/s}; v''=2:2000 \text{ m/s})$]. (b) Boltzmann plot from the integral population of the first three vibrational states of NO desorbing from $\text{Cr}_2\text{O}_3(0001)$ after LID with 6.4 eV for the two spin-orbit states $^2\Pi_{1/2}$ and $^2\Pi_{3/2}$ state.

the two spin-orbit states. The $^2\Pi_{1/2}$ state has a slightly lower vibrational population than the $^2\Pi_{3/2}$ state [Fig. 9(b)]. The reported populations are typical for laser induced nonthermal desorption and are similar to values found in a large number of other systems before.³

b. High coverage regime. So far, velocity distributions have been presented which are independent of the particular detection geometry and can be compared directly to theoretical calculations. However, such a transformation of TOF data into velocity distributions is only meaningful in case the rupture of the surface bond proceeds quasi instantaneous on the time scale of the time-of-flight spectra. This is mainly fulfilled for direct bond breaking. On the other hand, in case that trapping and diffusion on the surface or similar processes occur prior to desorption, the time required for the molecules to escape from the surface can be long compared to the flight time into the detection volume. In such a case, it is more appropriate to analyze the original spectra recorded as a function of time delay after the desorption pulse. As will be seen, the latter is the case for the high coverage regime so that both, velocity as well as time delay spectra will be presented.

Figure 10(a) shows velocity distributions for a selected rovibronic state ($J''=17.5, v''=0, ^2\Pi_{1/2}$) as a function of NO coverage. The steady state concentration during the experiment is controlled by the NO background pressure. The overall intensity desorbed per laser pulse increases with the background pressure compatible with the idea of a saturating monolayer of chemisorbed NO [Fig. 10(c)]. At low coverages, the velocity distribution is bimodal. With increasing coverage the slow channel is increasingly pronounced. The maximum of the distribution shifts significantly from 590 m/s (corresponding to a time delay of 54 μs) at a background dosing pressure of 3×10^{-10} Torr down to 200 m/s (160 μs) at 5×10^{-8} Torr. These velocities can formally be transformed into temperatures (via $T_{\text{trans}} = E_{\text{kin}}/2k_B$) resulting in 314 K which corresponds to 590 m/s and 36 K (200 m/s), respectively. The latter is a quite unphysical value as it appears rather unlikely that the mean translational temperature of the desorbing molecules is a factor of 3 smaller than the surface temperature. Obviously, other processes like diffusion or trapping retain NO molecules on the surface prior to their escape into the detection volume. Therefore, it is more appropriate to look at the spectra taken as a function of time delay after the desorption event as shown in Fig. 10(b).

From Fig. 10(b) it is apparent that the change in the overall shape of the delay time spectra occurs continuously within the whole range of NO coverages under investigation. This is in contrast to the TD spectra in which the weakly adsorbed species only appears after the chemisorption sites are saturated.

At time delays as long as 150 μs after the photoexcitation event, the rotational spectrum of desorbing NO still shows substantial rotational excitation. A rotational temperature of (500 ± 100) K is extracted from a Boltzmann analysis of the spectrum at this time delay. At a delay time of 800 μs , a rotational temperature of (400 ± 50) K was obtained. On one hand, this is much lower than for directly photodesorbed NO [$T_{\text{rot}} = (700 \pm 80)$ K]. On the other hand, the rotational

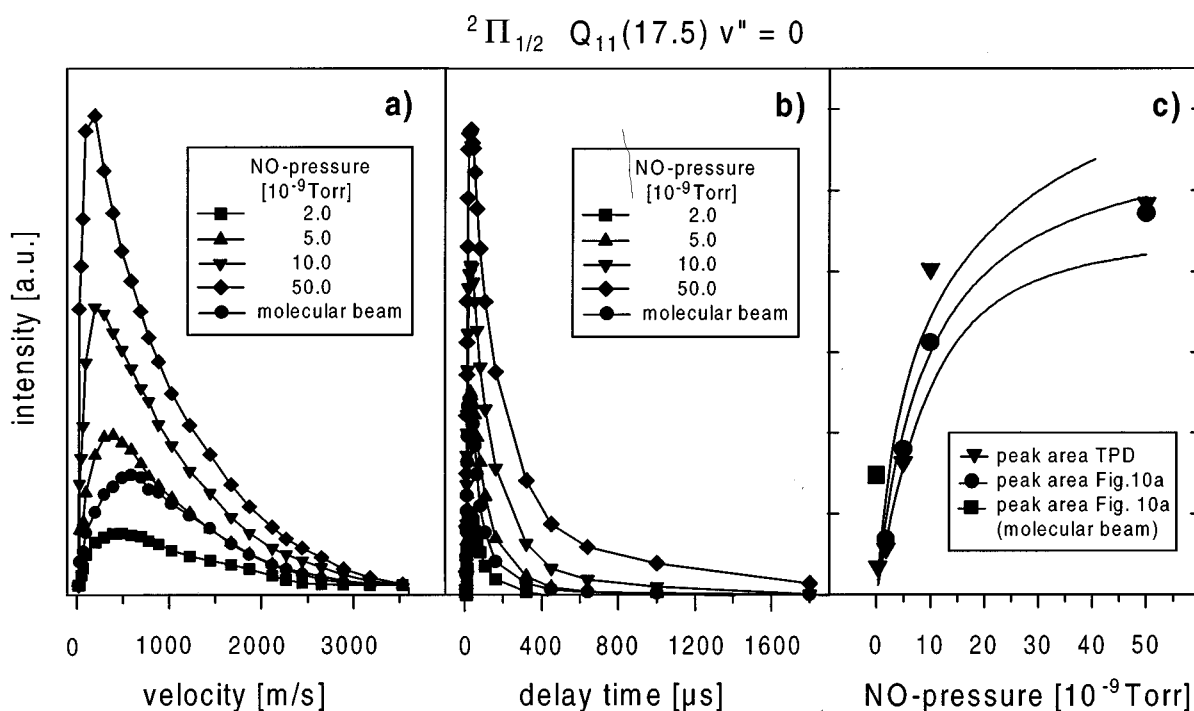


FIG. 10. (a) Velocity distributions as a function of background dosing pressure ($J''=17.5$, $v''=0$, ${}^2\Pi_{1/2}$) of NO desorbing from Cr₂O₃(0001) after LID with 6.4 eV, filled dots: molecular beam dosing (dosing at 4 Hz, driver pulse width 700 μs, NO stagnation pressure=2.0 bar, nozzle diameter=800 μm). (b) Corresponding original spectra as a function of time delay between desorption and detection event of (a). (c) Black dots: integrals of velocity distributions from (a) as a function of background dosing pressure. Black square: integral of velocity distribution from (a) of molecular beam dosing. Triangles: integrals of TPD spectra corresponding to velocity distributions from (a).

excitation is not fully accommodated to the surface temperature. It has to be noted that the drop in rotational excitation with increasing delay time is smooth.

IV. DISCUSSION

We have shown that NO adsorbs as a chemisorbed species at low NO coverages on Cr₂O₃(0001) with a binding energy of 1.0 eV. A weakly adsorbed species appearing at higher coverages is attributed to NO dimers with a possible bilayer like structure according to the IR data. The strong dimer bond is unusual. In the low coverage regime, conventional observations have been made for the UV laser (6.4 eV) induced desorption such as high vibrational and rotational excitation of desorbing neutral NO molecules exhibiting bimodal velocity distributions with strong coupling of translation to rotation. These findings are typical for a non thermal desorption process. Confirmed by further experiments¹⁸⁻²¹ this is conform with an initial charge transfer excitation of an electron from the substrate to the adsorbate to form an NO⁻ intermediate state. With this respect NO/Cr₂O₃(0001) is not different to a number of other adsorbate systems on similar oxidic supports as found experimentally and theoretically.^{3,7,8} However, the following unusual experimental observations have to be discussed for the high coverage regime:

(1) Slow components in the delay time spectra increase with increasing NO coverage for $v''=0$. They are related to retarded desorption after photoexcitation rather than being indicative to low kinetic energies. Residence times are found

to be up to several hundred microseconds before desorption. A smooth increase of delayed desorption with increasing coverage is in contrast to the TPD spectra in which dimers only appear once the chemisorption sites are saturated.

(2) The desorption cross sections depend on the desorption channel, on coverage, and internal degrees of freedom. The desorption probability drops at larger coverages for molecules evolving from a direct desorption process while no drop in desorption efficiency is observed for molecules with delayed desorption.

(3) The initial desorption signal per pulse is only proportional to the chemisorbate coverage for molecules from non retarded desorption. Furthermore, the question rises how is the dimer at higher coverage involved in the photoreaction?

The latter question has to be addressed as direct UV laser induced photodissociation of NO dimers has been demonstrated to be operative for (NO)₂ on LiF(001),³⁸ MgF₂ (Ref. 39) at 248 nm and cryogenic films on Ag(111) at 220–270 nm.¹¹ The NO fragments have been reported to occur in rather highly excited rotational and vibrational states. Dimer dissociation in the gas phase at 193 nm⁶⁴⁻⁶⁶ also showed substantial excitation of internal molecular degrees of freedom. However, in case of NO/Cr₂O₃(0001), neither a change in the population of internal degrees of freedom has been observed nor did the desorption signal per laser pulse increase with increasing coverage of the weakly bound species. Therefore, we exclude a nonthermal photodissociation of the dimers. This might arise either from the different type of dimer on Cr₂O₃(0001) compared to other systems and/or

a substantial shift of the resonance state with respect to the weakly adsorbed dimer.

If a direct nonthermal photodissociation of the dimer is to be ruled out, the question remains which mechanisms cause retarded desorption.

As relaxation processes of electronic or vibrational excitation are known to occur on a femtosecond and picosecond time scale,^{1-3,9} the long residence times of hundreds of microseconds after nanosecond excitation have to imply a long time diffusion process, in other words, mobility of the NO molecules along the surface plane after excitation. Momentum perpendicular to the surface needed for desorption then can be gained from collisions between the molecules. The presented results differ from other examples in the literature implying trapping or caging as normally the time for trapping is negligible with respect to the time scale of delay time spectra. Internal state populations are reported to be close to the surface temperature as typical for a preceding thermalisation process. Examples for this type of photodesorption mechanisms are NO desorption from multilayers of NO on Ag(111)¹¹ or from cryogenic films,¹² NO generated in substrate mediated photodissociation of NO₂ adsorbed on Pd(111)¹⁰ or NO desorbing after photodissociation of monolayers and multilayers of tert-butyl nitrate on Ag(111).¹³

Simple caging underneath further adsorbate layers can be ruled out for the NO/Cr₂O₃(0001) case for a further reason. The retarded desorption component in $v''=0$ is also apparent under experimental conditions for which only the chemisorbate state was observed in TPD and IR.

Photoinduced desorption involving collisions on the surface after photoreaction of adsorbed molecules has been reported for O₂/Ag(110).⁶⁷ For this system, photodesorption of O₂ is assumed to result from a two-step mechanism. Photodissociation of molecular oxygen is followed by collisions of hot oxygen atoms on the surface channelled along the rows of Ag(110) with unreacted molecules of initially zero kinetic energy. This collision is followed by desorption of translationally rather hot O₂ molecules.⁶⁷ A dramatic increase of the photodesorption cross sections with increasing O₂ coverage was explained by an increase of localized collisions. In our experiments differences of desorption efficiency are marginal. The difference might be a more efficient quenching of excited states and less channelled collisions in contrast to the O₂/Ag case.

The retarded desorption is only observed in $v''=0$. This indicates that vibrational excitation of the NO stretch is fully accommodated to the surface temperature for trapped molecules. Rotational excitation is not completely thermalised as is obvious, for example, from $T_{\text{rot}}=400$ K at 800 μs time delay between excitation and detection (distance of 32 mm from the surface). The elevated rotational temperatures rule out a pure thermal dissociation mechanism of dimers from a small laser induced temperature jump within the surface. For such a process, the rotational excitation would be expected to come close to the surface temperature.

The fact that a NO dimer forming a bilayer like structure is observed and the fact that desorption can occur after a longtime diffusion process without a complete rotational thermalisation strongly point to the involvement of an extrin-

sic precursor. The model for an extrinsic precursor in adsorption assumes that molecules adsorbed in a second layer are able to move freely until they reach a vacant adsorption site in the first layer and adsorb there.¹⁶

Therefore, we want to suggest the following speculative model for the desorption process. The NO is excited by an initial charge transfer from the substrate to the strong bound NO end in direct contact with the surface. This is consistent with the initial desorption signal per pulse being proportional to the chemisorbate coverage for molecules from nonretarded desorption. Direct desorption after backtransfer of the electron can occur and/or temporary trapping of hot molecules in an extrinsic precursor state results in a second desorption channel. The latter may be either from trapping of NO originating from the first layer in contact with the substrate or from NO molecules of the weakly bound second layer kicked off like billiard balls from the underlying excited chemisorbates. The trapped molecules have enough momentum to move freely parallel to the surface. They may collide with other molecules or they may be recaptured at a vacant chemisorption site in the first layer in contact with chromia. The more chemisorption sites are occupied the larger is the number of sites available in the second layer, i.e., sites for trapping. This can explain the drop in desorption probability for direct desorption. On the other hand, the probability for final recapturing of the molecules in the first layer will become smaller with increasing coverage. Furthermore, the necessarily increased collision rate within the second layer of mobile molecules will increase the probability to gain momentum perpendicular to the surface. Alternatively the rate for kicking off the physisorbed species which remain trapped for some time may increase. Both mechanisms are consistent with the increasing amount of delayed desorption.

Full rotational accommodation is not necessary for trapping in an extrinsic precursor state as found in scattering experiments for O₂/Ni(111) by Beutl, Rendulic, and Castro.⁶⁸ In other words, the molecule may rotate more or less freely which explains why it is not surprising to find elevated rotational temperatures for NO molecules desorbing after a long residence time from Cr₂O₃(0001).

V. CONCLUSIONS

We have shown for the first time to our knowledge the involvement of a precursor state in UV-laser induced desorption. Desorption was initiated at 6.4 eV for NO adsorbed at Cr₂O₃(0001) using nanosecond laser pulses at a substrate temperature of 100 K. At large coverages of NO, two desorption channels are observed: a direct one exhibiting strong translational, rotational, and vibrational excitation typical for initial charge transfer excitation within the adsorbate-substrate complex, and a second one characterized by retarded desorption with trapping times of several hundred microseconds. Within this second channel the internal degrees of freedom are thermalized to the substrate temperature except for the rotational excitation. The desorption probability for a direct desorption process is reduced in case the trapping channel gains importance. The data are interpreted assuming

that dimers observed at large coverages by IR spectroscopy forming a bilayer like structure act as extrinsic precursors within the desorption process.

It will be interesting to repeat UV laser induced desorption of adsorbates for which the existence of different precursor states have already been well established. Also scattering experiments for the system presented would be rather helpful to further confirm the existence of the suggested precursor state in the adsorption of NO on Cr₂O₃(0001).

The possibility that long time diffusion processes may also occur in photoreaction processes under certain conditions can have interesting consequences, for example, for limitations of surface structuring in an applied field like laser microfabrication.

ACKNOWLEDGMENTS

The authors should like to thank H. Kuhlbeck for helpful discussions concerning the infrared data and V. Staemmler for discussions on the desorption process. C. F. Friend is acknowledged for kindly sending the authors her manuscripts prior to publication. The Deutsche Forschungsgemeinschaft, the Ministerium für Wissenschaft und Forschung des Landes Nordrhein-Westfalen, and the Fonds der chemischen Industrie gave us financial support. KAS thanks the Ministerium für Wissenschaft und Forschung des Landes Nordrhein-Westfalen for a Lise-Meitner fellowship.

- ¹ *Laser Spectroscopy and Photochemistry on Metal Surfaces*, edited by W. Ho and H.-L. Dai (World Scientific, Singapore, 1993).
- ² F. M. Zimmermann and W. Ho, *Surf. Sci. Rep.* **22**, 127 (1995).
- ³ K. Al-Shamery, *Appl. Phys. A: Mater. Sci. Process.* **63**, 509 (1996).
- ⁴ D. Menzel, and R. Gomer, *J. Chem. Phys.* **41**, 3311 (1964).
- ⁵ P. A. Redhead, *Can. J. Phys.* **42**, 886 (1964).
- ⁶ P. R. Antoniewicz, *Phys. Rev. B* **21**, 3811 (1980).
- ⁷ T. Klüner, H.-J. Freund, J. Freitag, and V. Staemmler, *J. Chem. Phys.* **104**, 10030 (1996).
- ⁸ T. Klüner, H.-J. Freund, V. Staemmler, and R. Kosloff, *Phys. Rev. Lett.* **80**, 5208 (1998).
- ⁹ R. R. Cavanagh, D. S. King, J. C. Stephenson, and T. F. Heinz, *J. Phys. Chem.* **97**, 786 (1993).
- ¹⁰ E. Hasselbrink, S. Jakubith, S. Nettesheim, M. Wolf, A. Cassuto, and G. Ertl, *J. Chem. Phys.* **92**, 3154 (1990).
- ¹¹ W. C. Natzle, D. Padowitz, and S. J. Sibener, *J. Chem. Phys.* **88**, 7975 (1988).
- ¹² L. M. Cousins, R. J. Levis, and St. R. Leone, *J. Chem. Phys.* **91**, 5731 (1989).
- ¹³ H. G. Jenniskens, L. Philippe, W. van Essenberg, M. Kadodwala, and A. W. Kleyn, *J. Chem. Phys.* **108**, 1688 (1998).
- ¹⁴ J. A. Becker and C. D. Hartman, *J. Phys. Chem.* **57**, 157 (1953).
- ¹⁵ G. Ehrlich, *J. Phys. Chem.* **59**, 473 (1955).
- ¹⁶ P. Kisliuk, *J. Phys. Chem. Solids* **3**, 78 (1957).
- ¹⁷ *Kinetics of Interface Reactions*, edited by M. Grunze and H. J. Kreuzer, Springer Ser. Surf. Sci. **8** (Springer, Berlin, 1986).
- ¹⁸ M. Wilde, I. Beauport, K. Al-Shamery, and H.-J. Freund, *Surf. Sci.* **390**, 186 (1997).
- ¹⁹ M. Wilde, K. Al-Shamery, and H.-J. Freund, Proceedings of the SPIE'S OE/LASER '98 Conference, 1998, Vol. 3272, p. 152.
- ²⁰ M. Wilde, K. Al-Shamery, and H.-J. Freund (unpublished).
- ²¹ S. Thiel, T. Klüner, M. Wilde, K. Al-Shamery, and H.-J. Freund, *Chem. Phys.* **228**, 185 (1998).
- ²² M. Menges, B. Baumeister, K. Al-Shamery, H.-J. Freund, C. Fischer, and P. Andresen, *Surf. Sci.* **316**, 103 (1994).
- ²³ O. Seiferth, Ph.D. thesis, Bochum, 1997.
- ²⁴ D. C. Jacobs and R. N. Zare, *J. Chem. Phys.* **85**, 5457 (1986).

- ²⁵ F. Rohr, M. Bäumer, H.-J. Freund, J. A. Meijas, V. Staemmler, S. Müller, L. Hammer, and K. Heinz, *Surf. Sci.* **372**, L291 (1997); **389**, 391 (1997).
- ²⁶ P. A. Redhead, *Vacuum* **12**, 203 (1962).
- ²⁷ C. Xu, M. Hassel, H. Kuhlbeck, and H.-J. Freund, *Surf. Sci.* **258**, 23 (1991).
- ²⁸ C. Xu, Ph.D. thesis, Bochum, 1991.
- ²⁹ *Adsorption on Ordered Oxide Surfaces of Ionic and Thin Films*, edited by H.-J. Freund and E. Umbach, Springer Ser. Surf. Sci. **33** (Springer, Berlin 1993).
- ³⁰ M. Bender, D. Ehrlich, I. N. Yakovkin, F. Rohr, M. Bäumer, H. Kuhlbeck, H.-J. Freund, and V. Staemmler, *J. Phys.: Condens. Matter* **7**, 5289 (1995).
- ³¹ K. Nakamoto, *Infrared Spectra of Inorganic and Coordination Compounds* (Wiley, New York, 1963).
- ³² P. Hollins, *Surf. Sci. Rep.* **16**, 51 (1992).
- ³³ P. Hollins and J. Pritchard, *Prog. Surf. Sci.* **19**, 275 (1985).
- ³⁴ W. A. Brown, P. Gardner, and D. A. King, *J. Phys. Chem.* **99**, 7065 (1995).
- ³⁵ R. J. Behm and C. R. Brundle, *J. Vac. Sci. Technol. A* **3**, 1040 (1984).
- ³⁶ M. Perez Jigato, V. Termath, P. Gardner, N. C. Handy, D. A. King, S. Rassias, and M. Surman, *Mol. Phys.* **85**, 619 (1995).
- ³⁷ L. Sanche and M. Michaud, *J. Chem. Phys.* **81**, 257 (1984).
- ³⁸ R. C. Jackson, J. C. Polanyi, and P. Sjövall, *J. Chem. Phys.* **102**, 6308 (1995).
- ³⁹ C. J. S. M. Simpson, P. T. Griffiths, H. L. Wallaart, and M. Towie, *Chem. Phys. Lett.* **250**, 342 (1996).
- ⁴⁰ I. S. Nandhakumar, Z. Y. Li, R. E. Palmer, and R. Amos, *Surf. Sci.* **329**, 184 (1995).
- ⁴¹ E. L. Kugler, A. B. Kadet, and J. W. Gryder, *J. Catal.* **41**, 72 (1976).
- ⁴² A. Zecchina, E. Garrone, C. Morterra, and S. Colucchia, *J. Phys. Chem.* **79**, 978 (1975).
- ⁴³ G. Ghiotti, E. Garrone, G. Della Gatta, B. Fubini, and E. Giamello, *J. Catal.* **80**, 249 (1983).
- ⁴⁴ S. J. Conway, J. W. Falconer, and C. H. Rochester, *J. Chem. Soc., Faraday Trans. 1* **85**, 79 (1989).
- ⁴⁵ E. L. Kugler, R. J. Kokes, and J. W. Gryder, *J. Catal.* **36**, 142 (1975).
- ⁴⁶ E. L. Kugler and J. W. Gryder, *J. Catal.* **36**, 152 (1975).
- ⁴⁷ H. Kuhlbeck, *Appl. Phys. A: Solids Surf.* **59**, 469 (1994).
- ⁴⁸ C. E. Dinerman and G. E. Ewing, *J. Chem. Phys.* **53**, 626 (1976).
- ⁴⁹ S. G. Kukolich, *J. Am. Chem. Soc.* **104**, 4715 (1982).
- ⁵⁰ W. N. Lipscomb, F. E. Wang, W. R. May, and E. L. Lippert, Jr. *Acta Crystallogr.* **14**, 1100 (1961).
- ⁵¹ W. A. Guillory and C. E. Hunter, *J. Chem. Phys.* **50**, 3516 (1969).
- ⁵² J. Suzanne, J. P. Coulomb, M. Bienfait, M. Matecki, A. Thomy, B. Croste, and C. Marti, *Phys. Rev. Lett.* **41**, 760 (1978).
- ⁵³ V. M. Bermudez, *J. Vac. Sci. Technol. A* **10**, 152 (1992).
- ⁵⁴ O. Seiferth, K. Wolter, B. Dillmann, G. Klivenyi, H.-J. Freund, D. Scarano, and A. Zecchina (unpublished).
- ⁵⁵ V. Staemmler, in *Adsorption on Ordered Oxide Surfaces of Ionic and Thin Films*, edited by H.-J. Freund and E. Umbach, Springer Ser. Surf. Sci. **33** (Springer, Berlin, 1993), p. 169.
- ⁵⁶ J. R. Hertzler, M. P. Casassa, and D. S. King, *J. Phys. Chem.* **95**, 8086 (1991).
- ⁵⁷ P. Dumas, M. Suhren, Y. J. Chabal, C. J. Hirschmugl, and G. P. Williams, *Surf. Sci.* **371**, 200 (1997).
- ⁵⁸ K. T. Queeney, S. Pang, and C. M. Friend (unpublished).
- ⁵⁹ K. T. Queeney and C. M. Friend, *J. Chem. Phys.* **107**, 6432 (1997).
- ⁶⁰ K. T. Queeney and C. M. Friend, *Surf. Sci. Lett.* **414**, L957 (1998).
- ⁶¹ L. J. Richter, St. A. Buntin, D. S. King, and R. R. Cavanagh, *J. Electron Spectrosc. Relat. Phenom.* **54/55**, 181 (1990).
- ⁶² J. A. Goldsmith and S. D. Ross, *Spectrochim. Acta A* **24A**, 993 (1968).
- ⁶³ J. H. Bechtel, *J. Appl. Phys.* **46**, 1585 (1975).
- ⁶⁴ O. Kajimoto, K. Honma, and T. Kobayashi, *J. Phys. Chem.* **89**, 2725 (1985).
- ⁶⁵ Y. Naitoh, Y. Fujimura, O. Kajimoto, and K. Honma, *Chem. Phys. Lett.* **190**, 135 (1992).
- ⁶⁶ Y. Naitoh, Y. Fujimura, K. Honma, and O. Kajimoto, *Chem. Phys. Lett.* **205**, 423 (1993).
- ⁶⁷ Q.-S. Xin and X.-Y. Zhu, *Surf. Sci.* **347**, 346 (1996).
- ⁶⁸ M. Beutl, K. D. Rendulic, and G. R. Castro, *Surf. Sci.* **385**, 97 (1997).